International Scientific Journal
Environmental Science
http://environment.scientific-journal.com

Wind Farm Optimization based on CFD Simulation of Non-Flat Terrain

A.Bonanni*, T.Banyai†, Mehrdad Raisee‡, Dinesh Kumar§, J.VanBeeck¶, H.Deconinck‖, C.Lacor**
Von Karman Institute for Fluid Dynamics, Brussels, Belgium
Email: *bonanni@vki.ac.be, †banyai@vki.ac.be, ¶vanbeeck@vki.ac.be, ‖deconinck@vki.ac.be
Vrije Universiteit Brussel, Brussels, Belgium
Email: ‡mraiseed@vub.ac.be, §kumar@vub.ac.be, **chris.lacor@vub.ac.be
‡School of Mechanical Engineering, College of Engineering, University of Tehran, Iran

***Abstract*—Wind farm optimization defines the engineering problem of designing a wind farm with the objective of maximizing the energy production with respect to the operating costs. In the present work, a wind farm optimization model suitable for non flat terrains is presented. The proposed model combines an analytical model with a Computational Fluid Dynamics analysis.**

I. Introduction

Wind energy is one of the fastest growing businesses worldwide. Among the others it is also one of the most cost-effective alternatives to traditional energy production methods. The engineering challenge of exploiting the wind resources consists in maximizing the energy produced, keeping the wind farm costs (building and maintenance) at an acceptable level. Before building a wind farm, detailed information about the wind speed distribution (wind direction and intensity) are recorded over a period of several months. Once those information are available, the number and the position of the turbines is decided on the basis of a maximum energy-to-cost ratio. Complex phenomena like turbine wake interactions drive this phase. In fact, wind turbines produce energy according to the local wind speed and at the same time generate a wake that propagates downwind and interfere with the other turbines. A systematic approach for the wind farm design optimization problem can be first found in the work of Mosetti et al [1]. Several other works followed in recent years, confirming the interest towards the application both from an academic and an industrial point of view. In [2], an improved optimization process is set up (more individuals and more generations are used for the evolutionary algorithm). Emami et al. [3] use an improved objective function for the optimization process. Wan et al [4] first introduce a realistic wind speed distribution. All the works mentioned are based on a wake model to estimate the effect of the wind speed reduction behind each wind turbine. The wake model is required to be efficient since the computation of the velocity is performed many times during the optimization process. Many wake models have been developed over the years and one of the most widely used is the Jensen model [5]. One of the limitations of the Jensen model [5] is the assumption that the wind flow is homogeneous over the wind farm site and therefore is not suitable for the analysis of non-flat sites. The present work represents an attempt to extend the Jensen model to account for moderate non uniformities of the terrain topology. A CFD field is calculated before hand and is integrated into the Jensen model considering a one way coupling of the velocity field. A similar coupling technique applied to wind turbine wake models can also be found in [6]. Finally, a testcase based on an analytically derived terrain topology is set up to prove the concept.

II. Wind Farm Model

A. Single Turbine Model

The simplest way to estimate the wind flow field downstream of a wind turbine is by analytical models like the one proposed by Jensen [5]. This model is based on the momentum conservation and the variation of the speed is given by:

$$u = u_0 \left[1 - \frac{2a}{\left(1 + \alpha(d/r_1)\right)^2} \right] \tag{1}$$

where u_0 (in the original formulation) is the mean wind speed outside the wake, a is the induction factor, d the axial distance from the upstream turbine and α is the entrainment constant (see fig. 1). The wake radius downstream is given by:

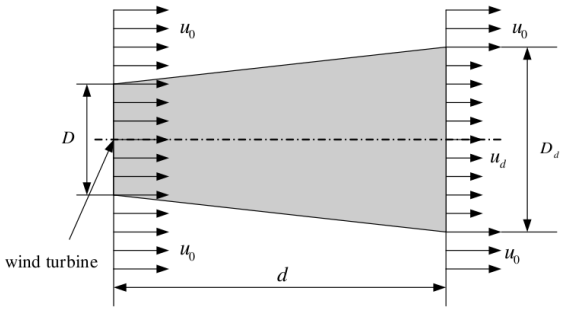

Fig. 1. Scheme of Jensen wake model ($D = 2r_{wt}$ and $D_1 = 2r_1$) [4].

$$r_1 = r_{wt}(1 + \alpha d) \tag{2}$$

The induction factor a is related to the wind turbine thrust coefficient C_T by the following relation:

$$C_T = 4a(1 - a) \tag{3}$$

The entrainment constant α is empirically found [1]:

$$\alpha = \frac{0.5}{\ln(z_{hub}/z_0)} \tag{4}$$

where z_{hub} is the wind turbine hub height and z_0 the terrain roughness. In the present work, the space variation of the wind speed is taken into account and therefore the assumption of constant wind speed over the domain is dropped. Equation 1 is modified introducing the velocity $u_0(x, y)$ variable in space. Equation 1 can be rewritten as:

$$u = u_0(x, y)\left[1 - \frac{2a}{(1 + \alpha(d/r_1))^2}\right] \quad (5)$$

The velocity field $u_0(x, y)$ is computed by the CFD simulation of the so called "background flow" (Section II-C), prior to the optimization algorithm. The background flow consists in the undisturbed wind velocity field over the terrain (measured at hub height). This way, a one way coupling between the Jensen wake model and the CFD flow is realized.

B. Wake interaction

The interaction of several wind turbine wakes is taken into account assuming that the kinetic energy loss at a specific wind turbine location is the sum of the energy losses obtained considering separately the effect of all the upstream wind turbines [7]. Therefore, the incoming wind speed at the location of the turbine i can be computed as:

$$u_i = u_i^U - \sqrt{\sum_{j=1}^{N_i}(u_j - u_{j,i})^2} \quad (6)$$

where u_i^U is the undisturbed wind speed (without wake effect) at the i-th turbine location, u_j is the wind speed at the location of the $j - th$ upstream wind turbine, N_i the number of turbines upstream the turbine i and $u_{j,i}$ the velocity at the location of the i-th turbine as if it were subject uniquely to the wake of the upwind turbine j-th. With respect to the original formulation [7], in this case the wind speed of the $j - th$ turbine and u_i^U are not assumed constant but rather computed by the CFD simulation of the "background flow" (Section II-C). Once the incoming wind speed is computed at each wind turbine location, the power output of each turbine P_{wt} can be computed as:

$$P_{wt} = \frac{1}{2}\rho U_{wt}^3 A C_P \quad (7)$$

where ρ is the air density, U_{wt} the wind speed at the turbine location, A the rotor area and C_P is the power coefficient that can be put in relation to the incoming wind speed U_{wt} by the C_P-curve provided by the wind turbine manufacturer (fig. 2): In this work, the approach of [1] and [2] is followed, where

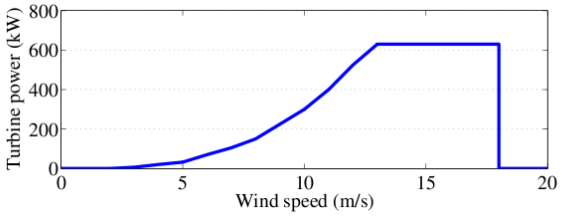

Fig. 2. Example of power curve of a 630Kw Turbine (reproduced from [4]).

P_{wt} is simply computed as $P_{wt} = 0.3U_{wt}^3$ (and neither cut-in nor cut-out speed limits are set).

C. CFD model of background flow

The wind over the wind farm location is based on a steady RANS computation of the $k - \epsilon$ turbulence model [8]. The numerical discretization of the set of non-linear differential equations is performed by a finite elements technique, employing a SUPG/PSPG (Streamline-Upwind Petrov/Galerkin, Pressure-Stabilized Petrov/Galerkin) spatial discretization [9]. The time integration is performed by Crank-Nicholson time-marching algorithm. Inlet profiles and wall-functions are the ones suitable for neutrally stable atmospheric boundary layers [10] [11].

D. Model Validation

In order to validate the proposed model, a testcase of a non-flat terrain is considered. The testcase consists of an analytically defined hill. The shape is defined by the following expression:

$$z(x, y) = h_m e^{-(r-r_0)^2/(2\sigma^2)} \quad (8)$$

where r is the distance from the center of the domain, r_0 the radius of the highest edge, h_m is the maximum height (set to 180 m) and σ is the variance given by:

$$\sigma = \begin{cases} 600\,m & r < r_0 \\ 200\,m & r > r_0 \end{cases}$$

It must be noted that the variance in the internal part of the highest edge is intentionally set to a higher value to guarantee a smoother and flatter internal part. This feature is desirable as it eliminates recirculation regions in the domain. The CFD

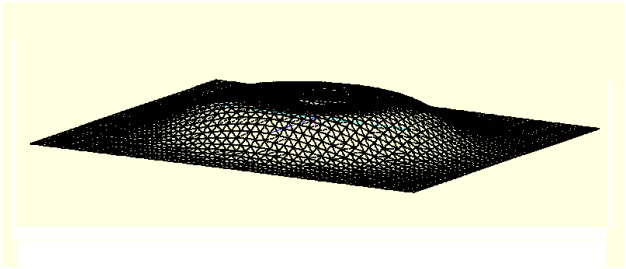

Fig. 3. Hilly terrain defined by exponential law.

mesh used to calculate the background flow is characterized by the parameters shown in Table I. The CFD simulations are

Domain size (m)	2000×2000×911.6
Nb Cells	144000
Nb Nodes	26896
First cell height (m)	2

TABLE I. SUMMARY OF CFD MESH DATA.

set up as follows:

- Inlet: the profiles as set according to [10]. The mean reference speed u_0 is set at the hub height h (equal to $60m$). The atmospheric turbulence intensity is set to 3% and the terrain roughness is $0.3m$.
- Bottom: wall functions as described in [11] are used.
- Top/Lateral: the velocity profile is set parallel to the boundary itself.

- Outlet: pressure assigned.

The velocity field calculated at hub height is depicted in figure 4 for the $u_0 = 12m/s$ simulation. Two wind turbines have

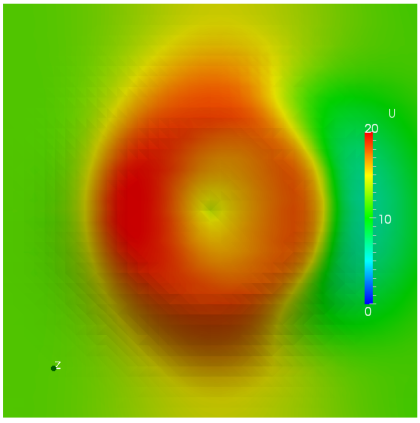

Fig. 4. Contour plot of Wind speed at hub height (Baseline).

then been added in the CFD domain by using an actuator disk model [12]. The wind turbine parameters are detailed in Table II. The velocity at hub height is depicted in figure 5.

Thrust Coefficient	0.88
Coordinates WT#1	x=700m, y=900m
Coordinates WT#2	x=1300m, y=900m
Hub height	60m

TABLE II. ACTUATOR DISKS PARAMETERS.

With respect to the baseline simulation, the mesh resolution has been increased around the actuator disks to better capture the wind speed drop. The overall length of the domain has also been increased to avoid the turbine wakes to interfere with the outlet boundary. The velocity profile at hub-height

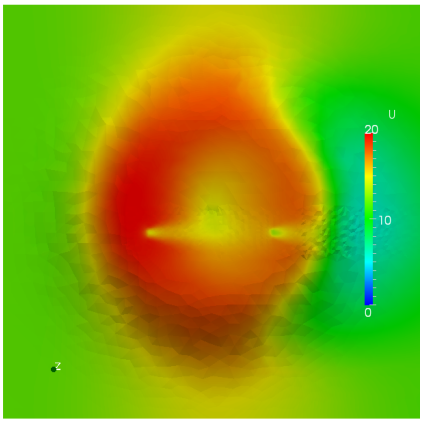

Fig. 5. Contour plot of Wind speed at hub height (with actuator disks).

has then been calculated by the analytical approach explained in section II. The comparison against the CFD simulation is shown in figure 6. Figure 6 shows that the velocity profile along the wind turbine line presents a velocity deficit with respect to the solution without wind turbines (baseline) due to the presence of the actuator disks. In between the two wind turbines (at approximately x=1000m) the velocity deficit with

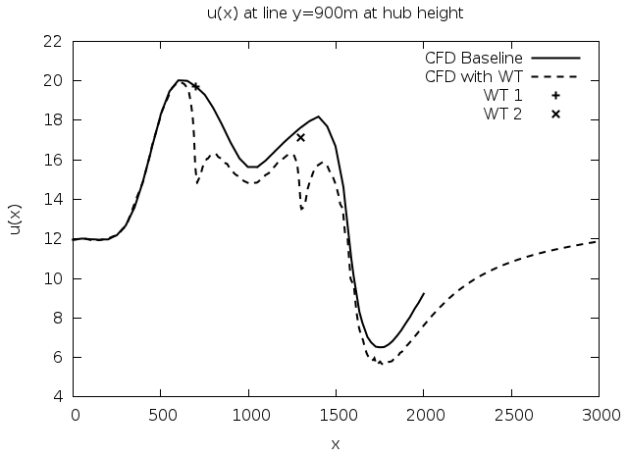

Fig. 6. Comparison between the analytical approach (Section II) and full CFD model with actuator disks.

respect to the baseline profile is approximately constant. The analytical model predicts a smaller velocity deficit, but capture this effect.

III. WIND FARM DESIGN

A. Problem formulation

The wind farm model used in this work is originally found in [1]. The same model has been reviewed and improved by several authors over the years [2] [3] [4]. It is defined by four different parts:

- Input parameters: Distribution of wind speed and direction, turbulence intensity, Wind turbines geometry, operating thrust coefficient, terrain roughness.
- Analytical wake model.
- Wake interaction model.
- Wind Farm power output and cost functions: Several models can be used both for power output and cost (they can easily be changed with more realistic data provided by the turbine manufacturer).

The following sections report the details of each of these parts of the wind farm model.

B. Input parameters

Concerning the input parameters, both the incoming wind speed and its distribution over the wind rose are assumed to be known. A distribution of wind speed magnitude can also be considered [4]. For the present work, both the wind speed and the wind direction are assumed to be normally distributed:

$$u = \bar{u} + \sigma_u \zeta_1, \qquad \alpha = \bar{\alpha} + \sigma_\alpha \zeta_2. \tag{9}$$

where $\bar{u}$ and $\bar{\alpha}$ are mean values of wind velocity and direction respectively, while σ_u and σ_α are standard deviations of u and α. ζ_1 and ζ_2 are two independent random variables normally distributed over the stochastic space $[-\infty, +\infty]^2$ with zero

i	j	H_{ij}	$< H_{ij}^2 >$
0	0	1	1
1	0	ζ_1	1
0	1	ζ_2	1
2	0	${\zeta_1}^2 - 1$	2
1	1	$\zeta_1\zeta_2$	1
0	2	${\zeta_2}^2 - 1$	2

TABLE III. 2D HERMITE POLYNOMIALS AND THEIR VARIANCES.

mean and a standard deviation of one. The joint probability density function is then expressed as:

$$pdf(\zeta_1, \zeta_2) = \frac{1}{2\pi} e^{-(\zeta_1^2+\zeta_2^2)/2} \tag{10}$$

The mean values and the variances are then used to calculate mean and variance of the total power output of the wind farm (Section III-D).

C. Wake model

The wake model used is described in sec. II. The analytical model is applied by considering that each wind turbine is affected by the wake of the upstream turbines and the wind speed deficit depends on the induction factor a (or Thrust coefficient C_T) and the mutual positions of the turbines.

D. Wind Farm Power Output

The total power output of the wind farm is calculated by considering the probability distribution of the wind speed and direction (eq. 9). Both the mean and the variance of the power output are used to build the objective function of the optimization problem. In order to calculate the mean and variance of the power output, a polynomial chaos (PC) expansion is used. The total power output of the wind farm P_{tot} is assumed to be a function of the reference wind speed u_0 and wind direction, α:

$$P_{tot} = P_{tot}(u_0, \alpha) \tag{11}$$

The polynomial chaos expansion of power, P_{tot}, is written as the summation over the multiplication of deterministic coefficients, P_{tot}^{ij}, and stochastic basis, H_{ij}, as:

$$P_{tot}(\zeta_1, \zeta_2) = \sum_{i,j=0}^{p} P_{tot}^{ij} H_{ij}(\zeta_1, \zeta_2), \tag{12}$$

where $H_{ij}(\zeta_1, \zeta_2)$ are 2D Hermite polynomials (Table III) and P_{tot}^{ij} are unknown coefficients that must be determined. The quadrature-based NIPC method uses spectral projection to find the NIPC expansion coefficients, P_{tot}^{ij}, in eq.12. Projecting eq.12 onto the k^{th} basis and using orthogonality gives:

$$P_{tot}^{ij} = \frac{1}{< H_{ij}^2(\zeta) >} \int_{-\infty}^{+\infty} \int_{-\infty}^{+\infty} I(\zeta_1, \zeta_2) d\zeta_1 d\zeta_2 \tag{13}$$

where,

$$I(\zeta_1, \zeta_2) = P_{tot}(\zeta_1, \zeta_2)\ H_{ij}(\zeta_1, \zeta_2)\ pdf(\zeta_1, \zeta_2) \tag{14}$$

In the quadrature-based NIPC method, the polynomial coefficients are obtained by evaluating the numerator in eq.13 numerically, while the denominator, $< H_{ij}^2(\zeta) >$, is computed analytically from multivariate orthogonal polynomials (See Table III). The 2-dimensional *Gauss-Hermite quadrature* can be used to compute the projection integral in eq.13. For the second order PC expansion ($p = 2$); the number of quadrature roots are $q = p + 1 = 3$. They are obtained by setting the third order Hermite polynomial $\zeta^3 - 3\zeta$ to zero. The three roots are: $\zeta^1 = -\sqrt{3}$, $\zeta^2 = 0$ and $\zeta^3 = +\sqrt{3}$. The corresponding weights for $p = 2$ are: $w_{q1} = 0.1667$, $w_{q2} = 0.6667$ and $w_{q3} = 0.1667$. In 2D extension, the number of quadrature points are $(p + 1)^2 = 3^2 = 9$ for a second order polynomial ($p = 2$). The locations of the quadrature points are shown in Fig. 7. The weights ($w_{q1} = 0.1667$, $w_{q2} = 0.6667$ and $w_{q3} = 0.1667$) and the value of the basis at $(\zeta_1^{i_1}, \zeta_2^{i_2}); i_1, i_2 = 1, 2, 3$ are known, therefore the total power is obtained by applying the algorithm explained in Section II-B and II-C for the 9 sample points of Table IV. This also implies running 9 CFD simulations of the background flow (Section II-C) at the wind speed and directions listed in Table IV. Finally, the statistical quantities of the stochastic function can be analytically derived from its PC expansion coefficients (eq.12). In particular, the mean and the variance respectively read:

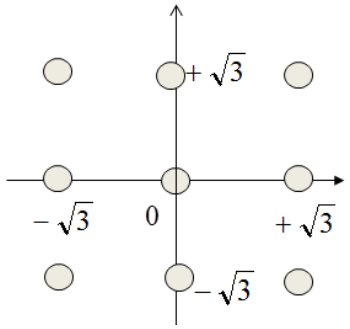

Fig. 7. Quadrature points in 2D stochastic space.

Run ID	u	α
#1	$\bar{u} - \sqrt{3}\sigma_u$	$\bar{\alpha} - \sqrt{3}\sigma_\alpha$
#2	$\bar{u} - \sqrt{3}\sigma_u$	$\bar{\alpha}$
#3	$\bar{u} - \sqrt{3}\sigma_u$	$\bar{\alpha} + \sqrt{3}\sigma_\alpha$
#4	$\bar{u}$	$\bar{\alpha} - \sqrt{3}\sigma_\alpha$
#5	$\bar{u}$	$\bar{\alpha}$
#6	$\bar{u}$	$\bar{\alpha} + \sqrt{3}\sigma_\alpha$
#7	$\bar{u} + \sqrt{3}\sigma_u$	$\bar{\alpha} - \sqrt{3}\sigma_\alpha$
#8	$\bar{u} + \sqrt{3}\sigma_u$	$\bar{\alpha}$
#9	$\bar{u} + \sqrt{3}\sigma_u$	$\bar{\alpha} + \sqrt{3}\sigma_\alpha$

TABLE IV. CFD RUNS FOR CALCULATING $P_{tot}(\zeta_1, \zeta_2)$ AT THE QUADRATURE POINTS.

$$\begin{aligned} \bar{P}_{tot} &= P_{tot}^{00}, \\ \sigma_{P_{tot}}^2 &= \sum_{\substack{i,j=0 \\ i+j\neq 0}}^{p} {P_{tot}^{ij}}^2 < H_{ij}^2 > \end{aligned} \tag{15}$$

The power output $\bar{P}_{tot}$ and its variance $\sigma_{P_{tot}}^2$ are then directly used in the objective function of the optimization algorithm (eq. 17).

E. Wind Farm Cost Function

Along with the power output mean and variance, it is also possible to include the cost of the energy produced into the model. To estimate the cost of the wind farm several cost models can be used. In this work, the model first used by Mosetti and Poloni [1] is adopted:

$$\mathcal{C} = N\left(\frac{2}{3} + \frac{1}{3}e^{-0.00174N^2}\right) \tag{16}$$

where N represents the total number of wind turbines installed.

IV. Optimization Methodology

A. Genetic Algorithm

To solve the optimization problem, the approach firstly introduced by Mosetti and Poloni [1] and later followed by many others [2] [3] [13] is here adopted. The wind farm is divided in a number of regular cells (10×10) where a wind turbine can possibly be placed (therefore the total number of turbines is not set beforehand, but is a result of the optimization algorithm). The goal of the optimization problem is to find in which cells to place the turbine in order to minimize the cost per unit of energy produced. The spacing of the cells is set to guarantee that each wind turbine does not operate in the near wake of the others (this is because in the near wake region both the velocity loss and the induced turbulence are deemed too high). In all the works mentioned, a square of $2km \times 2km$ is considered. If the wind turbine rotor diameter is set to $40m$, each turbine is spaced at least 5 diameters far from the others. If the wind farm is mapped on a 10×10 grid, the number of possible wind farm configurations is equal to 2^{100} which excludes the possibility of looking for the optimal solution by iterating over the configurations. Genetic algorithms can be applied in this case. Compared to other methods, they have the advantage of not requiring the knowledge of any derivative of the objective function and are less likely to get trapped into local minima. The idea behind evolutionary algorithms is to imitate the natural process of evolution through reproduction and probability of survival of the best individuals. The genetic information of each individual is represented by a chromosomal string that in the simplest case contains a sequence of 0's or 1's. The reproduction process is based on the generation of new chromosomes starting from the ones of two parents. Generation after generation, the evolution of the population is guaranteed by the higher probability of the fittest individuals to survive and generate new individuals. The evolution is essentially based on two different mechanisms: crossover and mutation. Crossover is the mechanism driving the production of new chromosomes by parents chromosomes. According to the crossover, the child chromosome receives part of the genetic information (0's or 1's in the chromosomal string) by one parent and part from the other parent. The probability of crossover is generally high (~ 0.8) and it is the process driving the local search for optimum. Mutation is the process that randomly introduces variations in the chromosomal string and its purpose is to avoid the population to sterilize and get trapped into local minima. The probability of mutation is much smaller and is generally of the order of ~ 0.01. Another mechanism that can be introduced is called "elitism" and means that the fittest individual (or individuals) of each generation are automatically transferred to the following generation. This avoids the loss of the best genomes reached by the population during the evolutionary process. In the present formulation of the problem, a single

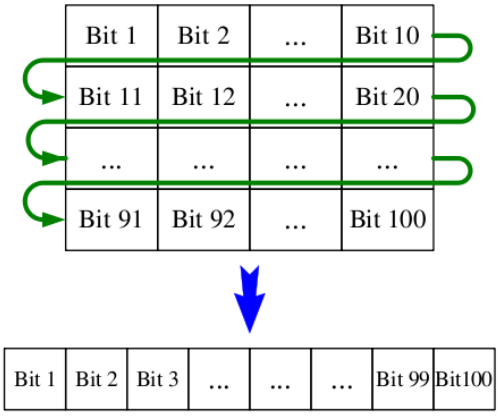

Fig. 8. Representation of the genome for a wind farm configuration (reproduced from [4]).

wind farm configuration is represented by a 10×10 matrix of 0's and 1's. Its genome is created by concatenating all its lines in a row 1×100 (fig. 8). The objective function $\mathcal{F}$ to minimize is defined as:

$$\mathcal{F} = w_1\bar{\mathcal{C}} + w_2\frac{1}{\bar{P}_{tot}} + w_3\frac{1}{\sigma^2_{\bar{P}_{tot}}} \tag{17}$$

where w_1, w_2 and w_3 are weight functions to give more importance to either the cost, power output or power output variance respectively. $\bar{C}$ is the cost adimensionalized by the cost of a wind farm with the maximum number of turbines installed (100 in this case) and $\bar{P_{tot}}$ the power of the wind farm adimensionalized with U_0^3.

V. Optimization Results

The optimization of the wind farm design is realized through the methodology explained in section IV. The optimization parameters are shown in table V. Figures 9 to 11 show

Nb of Individuals	800
Nb of Generations	2000
Crossover	0.95
Mutation	0.05
Mean Wind Speed [m/s]	12
Wind Speed variance [m/s]	1.15
Mean Wind Direction [deg]	270
Wind Direction variance [deg]	17.3
Wind Turbine Rad [m]	20

TABLE V. Optimization parameters.

the optimal configuration for three combinations of the weight coefficients of the objective function (eq. 17). The optimal wind farm configuration found by the evolutionary algorithm is in line with an intuitive best configuration (all the wind turbines are placed in the area with highest wind speed, around the hill circular top crest). It is worth noting that the testcase used here is intentionally simple to allow an easy interpretation of the optimal wind farm configuration. Figures 9 and 10 show

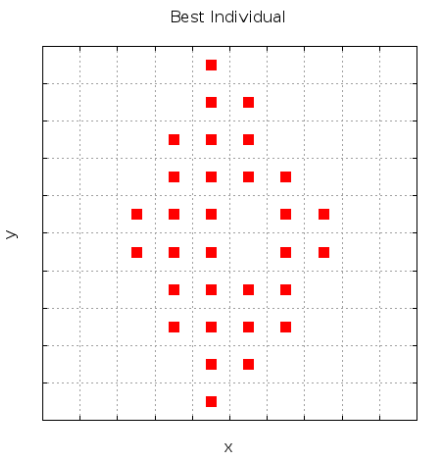

Fig. 9. Best wind farm configuration for $w_1 = 0.1$, $w_2 = 0.9$ and $w_3 = 0.0$

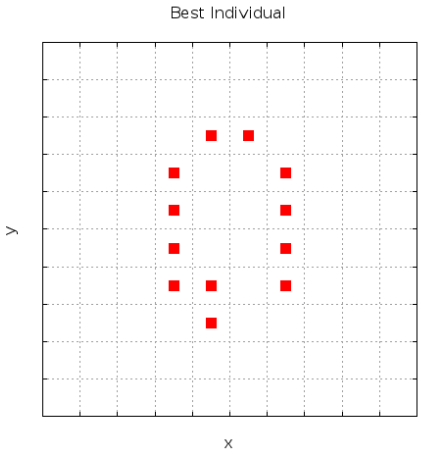

Fig. 10. Best wind farm configuration for $w_1 = 0.3$, $w_2 = 0.7$ and $w_3 = 0.0$

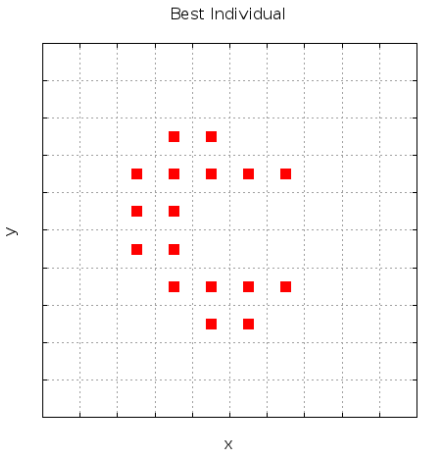

Fig. 11. Best wind farm configuration for $w_1 = 0.3$, $w_2 = 0.5$ and $w_3 = 0.2$

the influence of the cost of the wind farm on the optimal configuration. If the cost weighting factor w_1 is increased, the optimal configuration features fewer wind turbines. Figure 11 highlights the effect of considering the variance of the wind power output in the objective function. When the variance is taken into account in the objective function, the algorithm tends to promote a wind farm configuration with fewer wind turbines at the back of the hill crest. This can possibly reduce the wind farm power output drop due to the variation of wind direction and speed (comparison between figures 10 and 11).

VI. Conclusions

A wind farm analytical optimization model has been coupled with a CFD simulation of the undisturbed wind flow. The realized one way coupling allowed the solution of the wind farm optimization problem over a non-flat terrain represented by an analytically defined hilly terrain. The best wind farm layout found by the algorithm is in line with an intuitive solution, showing the effectiveness of the overall methodology. Further testing is required to explore more complex configurations.

Acknowledgments

I gratefully acknowledge the Von Karman Institute for Fluid Dynamics and the Vrije Universiteit of Brussels (VUB) for funding and supporting this research.

References

[1] G.Mosetti, C.Poloni, B.Diviacco, Optimization of wind turbine positioning in large wind farms by means of a genetic algorithm, Journal of Wind Engineering and Industrial Aerodynamics, 97 (1994) 105–116.

[2] S.A.Grady, M.Y.Hussaini, M.M.Abdullah, Placement of wind turbines using genetic algorithms, "Renewable Energy, Vol2-4" (2005) 259–270.

[3] A.Emami, P.Noghreh, New approach on optimization in placement of wind turbines within wind farm by genetic algorithms, "Renewable Energy, Vol35" (2010) 1559–1564.

[4] C. Wan, J. Wang, G. Y. X. Li, X. Zhang, Optimal micro-siting of wind turbines by genetic algorithms based on improved wind and turbine models, in: Joint 48th IEEE Conference on Decision and Control, Shanghai, China, 2009.

[5] N.O.Jensen, A note on wind generator interaction, Tech. rep., RISO Lab M-2411 (1983).

[6] A.Bonanni, T.Banyai, B.Conan, J.VanBeeck, H.Deconinck, C.Lacor, Wind farm optimization based on cfd model of single wind turbine wake, EWEA 2012, Copenhagen, 2012.

[7] C.T.Kiranoudis, Z.B.Maroulis, Effective short-cut modeling of wind park efficiency, "Renewable Energy, Vol2-4" (1997) 439–457.

[8] B.E.Launder, D.B.Spalding, Mathematical models of turbulence, Academic Press, London, 1972.

[9] T.Banyai, D. V. Abeele, H. Deconinck, A fast fully-coupled solution algorithm for the unsteady incompressible navier-stokes equations, Conference on Modelling Fluid Flow (CMFF06), 2006.

[10] P. Richards, R. Hoxey, Appropriate boundary conditions for computational wind engineering models using $k-\epsilon$ turbulence model, "J. Wind Eng. Ind. Aerodyn." (1993) 145–153.

[11] T.Banyai, A.Bonanni, T.Quintino, C.Lacor, H.Deconinck, Finite element technique for cfd simulations of atmospheric boundary layer flows, ICWE13, 2011.

[12] A.Bonanni, G.De.Volder, T.Banyai, T.Quintino, H.Deconinck, C.Lacor, Evaluation of turbine wake models in offshore wind farms, EWEC Offshore, Amsterdam, 2011.

[13] J.S.Gonzales, A.G.Rodriguez, J.C.Mora, J.R.Santos, Optimization of wind farm turbines layout using an evolutive algorithm, "Renewable Energy, Vol35" (2010) 1671–1681.